

# Unexplored Facet of Pincer Ligands: Super-Reductant Behavior Applied to Transition-Metal-Free Catalysis

Vikramjeet Singh, Rahul Singh, Arijit Singha Hazari, and Debashis Adhikari\*



Cite This: *JACS Au* 2023, 3, 1213–1220



Read Online

ACCESS |

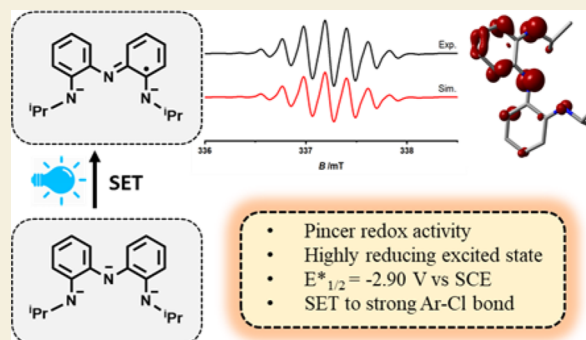
Metrics & More

Article Recommendations

Supporting Information

**ABSTRACT:** Pincer ligands are well-established supporting ancillaries to afford robust coordination to metals across the periodic table. Despite their widespread use in developing homogeneous catalysts, the redox noninnocence of the ligand backbone is less utilized in steering catalytic transformations. This report showcases a trianionic, symmetric NNN-pincer to drive C–C cross-coupling reactions and heterocycle formation via C–H functionalization, without any coordination to transition metals. The starting substrates are aryl chlorides that can tease the limit of a catalyst's ability to promote a reductive cleavage at a much demanding potential of  $-2.90$  V vs SCE. The reducing power of the simple trianionic ligand backbone has been tremendously amplified by shining visible light on it. The catalyst's success relies on its easy access to the one-electron oxidized iminosemiquinonate form that has been thoroughly characterized by X-band electron paramagnetic resonance spectroscopy through spectroelectrochemical experiments. The moderately long-lived excited-state lifetime (10.2 ns) and such a super-reductive ability dependent on the one-electron redox shuttle between the bisamido and iminosemiquinonato forms make this catalysis effective.

**KEYWORDS:** pincer, redox noninnocence, reductive cleavage, visible light redox, annulation



Pincers, a class of ligands affording tridentate coordination, have probably reached an iconic status in inorganic and organometallic chemistry.<sup>1–3</sup> Since the origin of organometallic complexes by tridentate coordination of pincer ligands in the late 1970s, it has witnessed a meteoric rise and has expanded its versatile applicability.<sup>4–6</sup> This category of ligands is extremely attractive due to their extensive modularity and tunability.<sup>7</sup> Furthermore, the ligand's robust chelating ability arises from the central coordinating motif. For example, pyridine would be lost under monodentate coordination mode, while it becomes reliably coordinated, as a part of the pincer backbone. Because of the rigid coordination architecture, sometimes, transition metal complexes bearing a pincer offer remarkable thermal stability, a property that is very much admirable in homogeneous catalysis affording molecular transformation at higher temperatures.<sup>8–10</sup> Having all these characteristics, pincers have been exploited to coordinate majority of metals ranging from the main group, transition metals, to lanthanides<sup>11</sup> across the periodic table. Moreover, metal–ligand cooperativity by designer pincers has been extensively exploited by Milstein's group to develop a large number of bifunctional homogeneous catalysts.<sup>12,13</sup>

Furthermore, pincers often enjoy extensive electron delocalization over multiple aromatic rings, which in turn decreases its highest occupied molecular orbital–lowest unoccupied molecular orbital gap. This property facilitates predominantly ligand-based filled and empty orbitals to

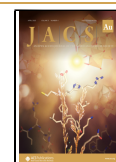
participate in redox processes under mild potential. Such features allow further redox tuning in the pincer backbone by minor modifications. Many pincers can shuttle between multiple redox states, accessing properties akin to redox reservoirs (Scheme 1).<sup>14</sup> Recently, such properties have also been utilized by Heyduk in advancing chemistry at the metal center where the electrons are mostly provided by the pincer ligand backbone.<sup>15,16</sup> Scrutinizing the three stable redox states separated by one-electron processes, we theorize that electron transfer catalysis might be possible by free ligands, (NNN)H<sub>3</sub>, I itself, without further assistance of the metal (Scheme 1b). We select this NNN pincer backbone that has been used earlier by Heyduk because of its ready access to the trianionic form.<sup>14</sup> The electron-rich nature of the symmetric NNN pincer in its fully deprotonated trianionic form may make it moderately reducing. However, the reducing property can be considerably amplified if the molecule is excited by shining visible light. The conjugated nature of the diarylamido backbone helps further light absorption within the visible

Received: February 15, 2023

Revised: March 27, 2023

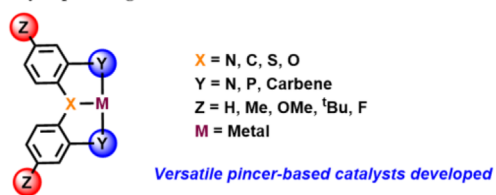
Accepted: March 28, 2023

Published: April 10, 2023



## Scheme 1. Scope for the Pincer Ligand's Noninnocence

## (a) Tunability in pincer ligand



## (b) Redox states afforded in an NNN-pincer ligand



range of electromagnetic spectra so that the excitation of the pincer becomes fully feasible under mild conditions. Leveraging this favorable redox, we harness the trianionic pincer in electron transfer catalysis and show that such a pincer can function as a super-reductant, a facet that has never been interrogated.

Examples of direct participation of pincers via electron transfer reactions from the ligand's backbones to promote molecular transformation are limited. Herein, we showcase such an electron transfer reaction from the pincer backbone without any assistance of transition metals. Much intriguingly, the trianionic NNN-pincer (**2**) under visible light excitation is super-reducing species that can reductively cleave even a C–Cl bond in *p*-methoxy chlorobenzene ( $E_{\text{red}}^{\circ} = -2.90$  V vs SCE).<sup>17</sup> It is further shown that this unprecedented electron transfer catalysis by pincer can forge a plethora of value-added heterocyclic products from substituted chlorobenzenes.

## RESULTS AND DISCUSSION

To demonstrate the pincer's electron transfer ability, we have chosen the trianionic NNN-pincer (**2**) so that the parent trisamido and its one-electron oxidized iminosemiquinonate form can be accessed readily. The stability of both redox states avoiding any detrimental bond cleavage in the pincer's backbone ensures this proposed redox to be viable. As can be anticipated, the trianionic backbone can be oxidized at an extremely mild potential. The cyclic voltammetry analysis of the trianion **2** exhibits the first reversible oxidation wave at  $-0.25$  V vs  $\text{Fc}^+/\text{Fc}$  couple. A second quasi-reversible oxidation is further observed at  $+0.04$  V (vs  $\text{Fc}^+/\text{Fc}$ ), (Figure S1, SI). For the sake of comparison, we convert the first oxidation potential with respect to SCE which is found to be  $0.13$  V.<sup>18</sup> Such a mild potential indicates easy oxidation and promises the molecule to be a potent reductant. We envisage that this reductive behavior can be tremendously augmented once the molecule is excited with visible light. To our advantage, the diaryl amido linkage absorbs significantly in the visible range of electromagnetic spectra. Having the possibility of photoexcitation of the pincer **2**, we delved into investigating its redox and basic photochemical properties. Upon scrutinizing through UV–visible spectroscopy, it is observed that the molecule absorbs at 335 and 392 nm, and the second maximum is connected to broad

absorption up to 455 nm (Figure S2, SI). Furthermore, **2** is photoactive and shows an emission band at 415 nm (Figure 1a), when excited at a wavelength of 380 nm. The molecule is

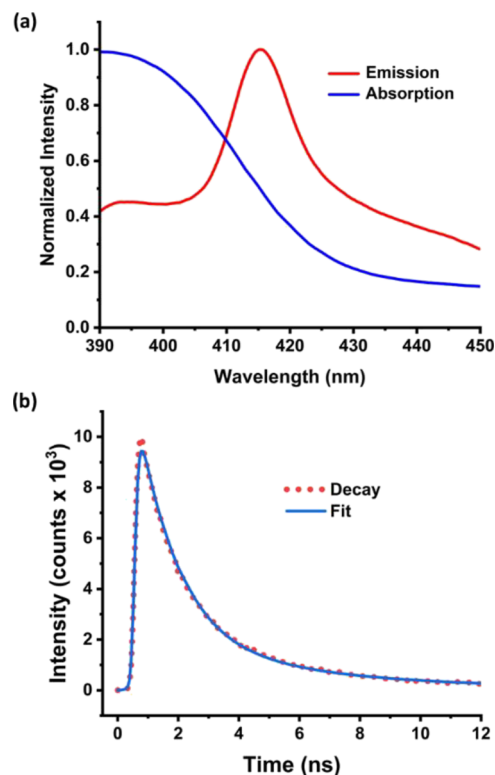


**Figure 1.** (a) Normalized absorption and emission spectra of **2** in THF. (b) Tri-exponential fit of TCSPC data of **2** collected at its emission maxima when excited with a 380 nm laser pulse. Data were recorded in dry and degassed THF using 1% ludox as the probe.

brightly fluorescing and this trait makes it propitious as a photocatalyst. However, efficient electron transfer from the excited state requires the same to be relatively long-lived.<sup>19</sup> To determine the excited state lifetime for **2**, a time-correlated single photon counting (TCSPC) measurement was performed. The decay of the fluorescence intensity was fitted with a triexponential function ( $\chi^2 = 1.24$ ) and the average fluorescence lifetime of the fluorophore was calculated as 10.2 ns (Figure 1b). The moderately long lifetime further assures the electron transfer to be fully feasible from its excited state.<sup>20</sup> This set of photophysical data also helps us to calculate the excited-state oxidation potential of **2**. The excitation energy ( $E_{\text{o,o}}$ ) of the molecule was estimated as 3.03 eV as derived from the intersection point of absorption and fluorescence spectral data. Accordingly, the excited-state oxidation potential by the Rehm–Weller equation<sup>21</sup> can be calculated as  $E_{\text{ox}}^* = E_{\text{ox}}^{\circ} - E_{\text{o,o}}$  and the value appears as  $-2.90$  V (vs SCE) (see the SI). Such a large negative value of the excited-state oxidation potential promises the molecule to be an extremely strong photo-reductant and will be able to reductively cleave the difficult-to-reduce bonds.<sup>22</sup>

Since electron removal from the bisamido form will generate the iminosemiquinonate form, we wanted to gather some spectroscopic signature for this redox state. The detection of one-electron oxidized form of **2** will generate further credence for such electron transfer, on which a catalytic process can be built. Along this direction, we performed a spectroelectro-

chemical EPR experiment (at  $-40\text{ }^{\circ}\text{C}$ ), which resulted in the detection of a complex pattern with a central g-value of 2.0043 (Figure 2a). Moreover, the experimentally observed spectrum

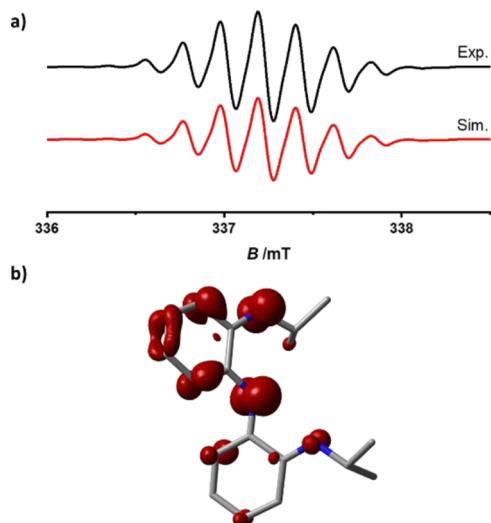


**Figure 2.** (a) X-band (9.46 GHz) EPR signal for the iminosemiquinonate form of **2** collected at  $-40\text{ }^{\circ}\text{C}$ . (b) Excess  $\alpha$ -spin density distribution for the same, calculated using the M06-2X/6-31G\* level of theory (iso value  $0.004\text{ (e bohr}^{-3})^{1/2}$ ).

was successfully simulated considering the two nitrogens which can be hyperfine-coupled and found the coupling parameters to be 11 and 6 MHz, respectively. From this spectroelectrochemistry experiment, it appears that the radical in the iminosemiquinonate form is more centered in one of the arylamido rings.

Though rather surprising, the same picture is quite reproducible from high-level DFT calculations. The iminosemiquinonate form of **2** was optimized at the M06-2X/6-31G\* level of theory<sup>23</sup> and was analyzed further to trace the locus of the unpaired spin. Gratifyingly, the spin density calculation on the monooxidized product depicts the excess spin to be delocalized on one of the aryl amido rings (Figure 2b). We reason that the lack of a complete delocalization onto the second ring may stem from the distortion of one aryl unit from the other aryl ring of the bisarylamido motif. In closer inspection, the two aryl rings are distorted out of plane at least by  $18^{\circ}$  to avoid the steric clash of ortho hydrogens at the two aryl units. In essence, detection of the one-electron oxidized product from **2** strongly supports the fact that the electron-rich trianionic backbone can facilitate electron transfer and generate a reasonably stable intermediate form.

### Catalytic Reactions

To explore the promised super-reducing behavior for the trianionic NNN pincer ligand **2**, we chose substituted chlorobenzene as a model substrate, where the reductive cleavage of the C–Cl bond poses a significant challenge.<sup>24</sup> Sometimes, such bond cleavages demand drastic conditions of using UV light<sup>25,26</sup> that is carcinogenic. The C–Cl bond is very difficult to cleave primarily owing to its bond strength and demands for a strong negative reduction potential.<sup>27</sup> The approach of generating a super-reducing excited state is very much suitable for the activation of carbon–halogen bonds in aryl chlorides for the following reasons: (a) Aryl chlorides do not absorb in visible light so that direct excitation is not

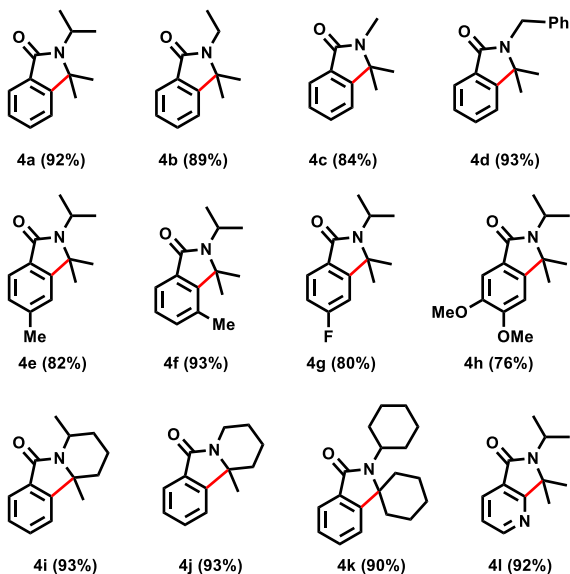
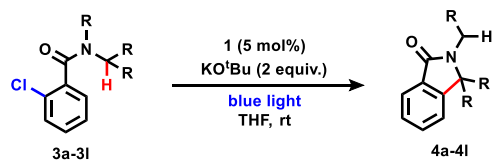
possible. (b) Their high reduction potentials are beyond the domain of many readily available and extremely popular photocatalysts such as  $[\text{Ru}(\text{bpy})_3]^{2+}$ ,  $\text{Ir}(\text{ppy})_3$ , and  $[\text{Ir}(\text{ppy})_2(\text{dtbbpy})]^+$ .<sup>28</sup> (c) Strong carbon–halogen bonds and their two-step bond dissociation kinetics can deter very good electron donors to cleave the bond requiring longer reaction times.<sup>29</sup>

To prove that **2** can perform productively under visible light excitation, we selected 2-chloro-*N,N*-dialkylbenzamide as a model substrate so that reductive cleavage of the aryl chloride bond can lead to the construction of an isoindolinone ring.<sup>30</sup> Upon extensive optimization, it was revealed that 5 mol % of the catalyst **1** can convert the chloro-substituted benzamide into the corresponding isoindolinone in 95% gas chromatography (GC) yield, with the use of 2 equivalent of base  $\text{KO}^t\text{Bu}$  (see Table S1, SI). Other bases such as DABCO and  $\text{K}_2\text{CO}_3$  are completely ineffective, while  $\text{NaO}^t\text{Bu}$  affords the product in 55% yield. Significant reduction in yield when  $\text{NaO}^t\text{Bu}$  is used as a base indicates the possible role of a counter cation on the reaction. It is notable that during this reaction, **2** is formed in situ by the deprotonation of the protonated precursor **1** so that stringent inert condition handling of **2** can be safely avoided. Instead, packing the bench-stable **1** in the reaction flask and purging the solution with nitrogen are adequate. The optimization further discloses that blue light is the most suitable photon source, while white light gives a lower yield of the product. The reaction is completed within 12 h of reaction time. Separate experiments in absence of light, catalyst **1**, and base prove that all these components are critical for the success of the reaction. Among different solvents, THF remains ideal. Isoindoline formation is an ideal demonstration of  $\text{C}(\text{sp}^2)\text{-H}$  functionalization using photoredox processes which is a nice alternative to classical transition-metal catalyzed C–H bond activation by concerted metalation and deprotonation.<sup>31–33</sup> To ensure that the reaction is not facilitated by adventitious transition metals, we performed the reaction in new glassware along with an unused stir bar. The product yield was very much reproducible under such test reactions. Attempts to detect any trace metal contamination in the used  $\text{KO}^t\text{Bu}$  also resulted in negative observations (see the SI for details).

Having the optimized condition in hand, we set out to test the scope of the reaction. The substrate 2-chloro-*N*-isopropyl-*N*-alkylbenzamide (**3a**) reacted selectively to result *N*-isopropyl isoindolinone ring **4a** in very high, 92% isolated yield (Table 1). Further substrate scope expansion facilitated the formation of **4b–4d** in high yields of products where the substitution of nitrogen was changed. Notably, the reaction is very selective to the activation of the isopropyl group connected to nitrogen sparing methyl or even benzyl groups. As will be discussed in the following section, this stems from the stability of the tertiary carbon radical that results from the hydrogen atom abstraction from isopropyl C–H. Methyl substitutions at the benzamide ring were tolerant to the reaction condition so that isoindolinone **4e** and **4f** can be forged in 82–93% isolated yields. Interestingly, a halide substituent like fluoride also afforded the respective isoindolinone **4g** in 80% isolated yield.

Electron-donating methoxy substituents were examined further which afforded 5,6-dimethoxy-*N*-isopropyl isoindolinone, **4h** in 76% yield. More sophisticated isoindolinone architectures can also be fabricated by this method as two heterocycles **4i** and **4j** were synthesized in very high, 93% yields. If the nitrogen substituents in the benzamide are

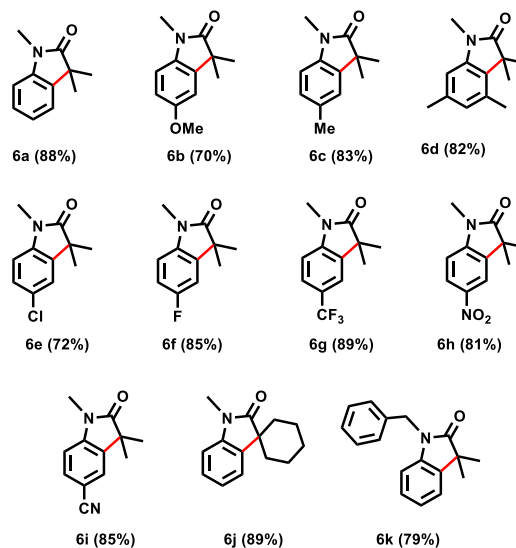
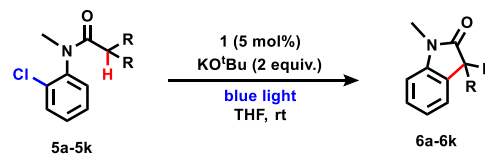
**Table 1. Scope of Intramolecular C–H Arylation of *o*-Chloro-*N,N*-dialkylarylamides**



cyclohexyl rings, the appropriate C–H functionalization affords the spirocyclic product **4k** in 90% yield. Notably, such spirocyclic isoindolinone is a valuable heterocyclic motif that can improve lipophilicity, aqueous solubility, and metabolic stability.<sup>34</sup> Finally, a heterocyclic ring pyridine was examined as a substrate that afforded the corresponding cyclized product **4l** in 92% yield. The high yield of products in reasonable reaction time makes pincer **1** a rival for the iridium photocatalyst that was utilized earlier to forge isoindolinone under photothermal reaction conditions.<sup>35</sup> Further advantage of our method over the previous iridium-based protocol is that high temperature is not a need.

After this, we sought to examine *N*-substituted *o*-chloroanilide as a potent substrate so that a C–Cl bond can be cleaved, and the subsequent cyclization can lead to value-added oxindole rings. The oxindole framework bearing a tetrasubstituted carbon center at the 3-position is regarded as a privileged motif that is often found in the core of a large class of bioactive natural products as well as pharmaceutically important compounds.<sup>36–38</sup> Accordingly, *o*-anilide arylchloride was tested under the same reaction conditions to afford 3,3-dimethyl oxindole **6a** in 88% yield (Table 2). Electron-donating methoxy or methyl substituents in the *o*-anilide aryl ring survived well through the reaction conditions to furnish products **6b–6d** in 70–83% yields. Notably, synthesis of 3,3-dialkyloxindole was earlier attempted from the aryl iodide substrate, where a precious metal photocatalyst *fac*-Ir(ppy)<sub>3</sub> was employed.<sup>39</sup> In case of 2,4-dichloro anilide molecules, the *o*-chloro group was selectively cleaved to provide **6e** in 72% yield. Likewise, highly electron-withdrawing trifluoromethyl group afforded 89% yield of the oxindole **6g**. Highly interestingly, a nitro substituent in the aryl ring was tolerant to the reaction condition and prepared the heterocycle **6h** in

**Table 2. Scope of Intramolecular C–H Arylation of *N*-(*o*-Chloroaryl)-*N*-methylalkylamide**



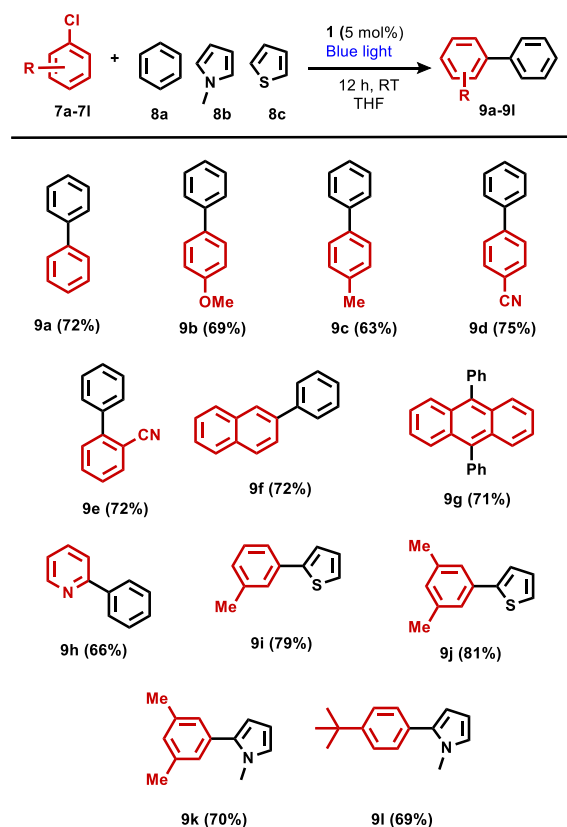
81% yield. Pharmaceutically important spirocycle **6j** and *N*-benzylated oxindole **6k** were also obtained by this method in excellent yields.

The visible-light-induced radical reaction has to date been limited to suitably activated haloarenes possessing a C(sp<sup>2</sup>)-X bond adjacent to a pi-system, such as  $\alpha$ -carbonyl, benzyl, or heteroatoms (halogen, oxygen).<sup>40–42</sup> To examine the full potential of the highly reducing excited state of **2**, we chose a few unactivated aryl chlorides. To this end, we examined a recalcitrant *p*-methoxy aryl chloride whose reduction potential to cleave the C–Cl bond is demanding  $-2.90$  V vs SCE was examined that afforded the respective biphenyl **9b** in 69% yield. Interestingly, 9,10-dichloro anthracene was an effective coupling partner so that two phenyl groups can be easily installed at the respective positions to give 9,10-diphenyl anthracene **9g** in 71% yield. A pyridyl ring was tolerant to the reaction condition to afford product **9h** in moderate, 66% yield. Additionally, aryl chlorides involving thiophene and *N*-methyl pyrrole as substrates afforded the C–C cross-coupled product **9i–9l** in 69–81% yields. The three different classes of the reaction, starting from varying strengths of aryl chloride bonds, attest the tremendous reducing power of the excited **2** and to steer subsequent ring cyclization or cross-coupling reactions.

Upon exploring the scope of the pincer ligand's strong photoreduction ability, we sought to gain more insight into the mechanistic details of the C–Cl cleavage reaction. As the reaction involves radicals, we performed a radical quenching



**Table 3. Cross-Coupling Reaction of Benzene, *N*-Methylpyrrole, and Thiophene with Aryl Chlorides**



experiment with TEMPO. As expected, the reaction completely shuts down upon addition of TEMPO in 1.0 equivalent. Moreover, as a compelling evidence to the aryl radical generation, *p*-OMe aryl radicals were successfully intercepted as its TEMPO adduct. The adduct was detected by high-resolution mass spectrometry (section 8, the SI). As already discussed, the highly reducing excited state of **2** (having  $E_{ox}^* = -2.90$  V vs SCE) is capable of cleaving an unactivated C–Cl bond of aryl chloride. To unambiguously prove that the electron transfer happens at the excited state of

**2**, we performed a Stern–Volmer luminescence quenching experiment. Gratifyingly, fluorescence intensity of the photocatalyst gradually decreased with increasing concentration of aryl chloride and such a decrease generated a clear straight-line pattern from the Stern–Volmer plot (Figure 3a). Incorporating the lifetime of the fluorophore, that has been measured earlier, we calculated the electron transfer rate as  $2.74 \times 10^9$   $M^{-1} s^{-1}$ . The electron transfer rate constant suggests the process to be only limited by diffusion of the quencher and the fluorophore. In comparison, a previous photocatalyst CzE-PAIPN $\cdot^-$  transfers electrons to aryl chloride at a rate of  $1.5 \times 10^7$   $M^{-1} s^{-1}$ .<sup>22</sup> When compared, the electron transfer rate in our chosen pincer backbone is two orders of magnitude faster that also likely reflects in the reduced reaction time (12 h). Taken the photophysical and redox properties of the photocatalyst molecule together, we delineate the reaction mechanism for the annulation reaction upon C–H functionalization. The photoexcitation of **2** prompts the electron transfer to rupture the C–Cl bond, generating an aryl radical. It is expected that losing one electron from the system will generate a dianionic radical, which is moderately stable that likely reflects in its extremely mild first oxidation potential. Notably, the electron transfer from the pincer backbone is reminiscent of Murphy's super electron donors, although those worked under stoichiometric conditions.<sup>46,47</sup>

The radical anion of Ar–Cl dissociates into an aryl radical, which undergoes a 1,5-hydrogen atom transfer (HAT) process.<sup>48–50</sup> In general, the 1,5-HAT processes are favored over 1,6-HAT because of their optimum chairlike six-membered cyclic transition state, thus favoring the annulation in this mode.<sup>51</sup> The newly generated alkyl radical **11** after HAT attacks the aryl ring to generate an intermediate **12** (Figure 3b). In the presence of a strong base KO<sup>t</sup>Bu, deprotonation can pursue to leave a radical anion of this species which is a strong reductant to give the electron back to the iminosemiquinone form of the photocatalyst to bring back the bisamido form. Therefore, the facile redox interconversion between bisamido and iminosemiquinone helps run the catalytic cycle. It is also notable that **2** essentially pushes the limit of accessible reduction potential to break the electron-rich aryl chloride bond. Earlier important discoveries including sensitization-induced electron transfer (SenI-ET)<sup>52</sup> or consec-

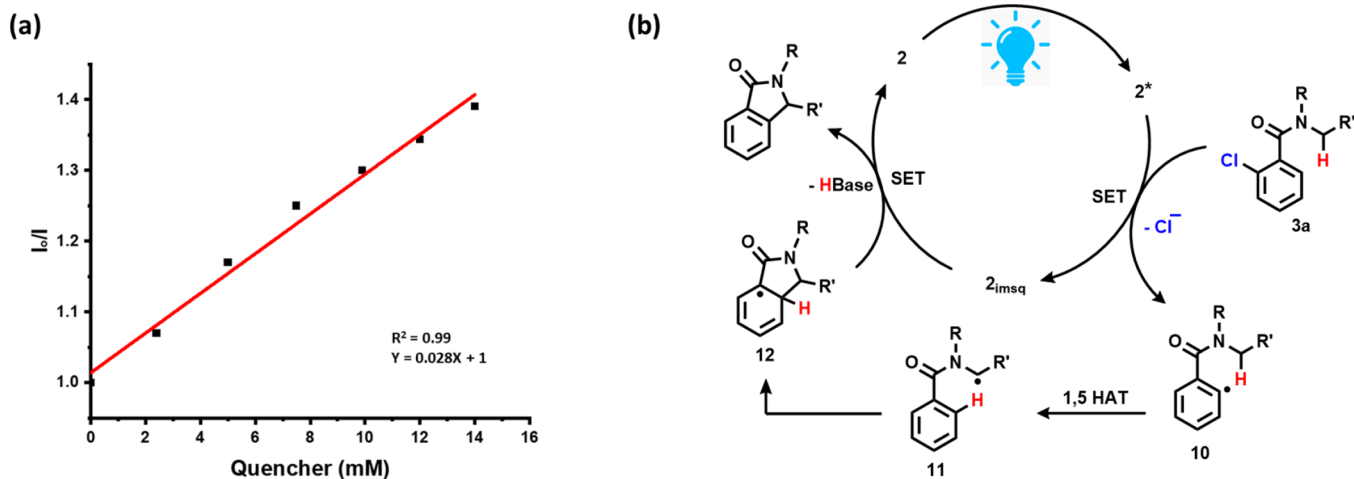


**Figure 3.** (a) Stern–Volmer plot for electron transfer from **2\*** to the 2-chloro-*N*-isopropyl-*N*-alkylbenzamide substrate. (b) Plausible mechanistic cycle under photoexcitation.

utive photoinduced electron transfer (ConPET)<sup>53</sup> have attempted to breaking strong bonds. Although conceptually seminal, majority of the ConPET catalysts effectively cleaved electron-poor aryl chlorides.<sup>54</sup> Our report shows that a simple anionic pincer can strategically reach such a limit upon visible light excitation. We were further curious about the fate of the pincer photocatalyst and inquired whether such radical generation in the backbone may lead to an N-isopropyl bond cleavage. Such bond rupture would be detrimental to the catalyst longevity. At the end of the reaction and standard work-up, when we analyzed the solution through GC–MS, we identified the protonated pincer backbone. This observation indicates that catalyst molecules remain intact at the end of the cycle. However, the challenging separation of the catalyst from the homogeneous solution mixture and our inability to quantify the amount of protonated ligands does not completely refute some possibility of the N-alkyl bond cleavage.

## CONCLUSIONS

In summary, we have unraveled a completely new aspect of a trianionic pincer ligand, where the electron-rich pincer steers electron transfer to substrate molecules. This is a rare report where the NNN pincer backbone can drive a strong bond cleavage and subsequent C–H functionalization without any assistance of a transition metal ion. The excited state of the molecule can be easily reached by shining blue light upon it. The molecule is an extreme photoreductant that is capable of reductively cleaving even very electron-rich aryl halides, essentially pushing the limit of a strong bond cleavage. Following this protocol, we have synthesized a wide array of benzannulated rings under mild reaction conditions and short reaction times. This reduction became possible due to the easy access of the two redox states by the pincer, whose important intermediate form has been detected spectroscopically. We believe that direct redox participation of many such ligands will surface in future where their redox properties can be modulated by shining visible light, and a tremendous amount of chemistry can be developed even under metal-free conditions.

## METHODS

### Materials

All operations were carried out in flame-dried glassware using a N<sub>2</sub>-gas-filled glovebox or high-vacuum standard Schlenk techniques under a nitrogen gas atmosphere unless mentioned otherwise. THF was refluxed and freshly distilled over sodium/benzophenone and degassed using three freeze–pump–thaw cycles. Starting materials and reagents were purchased from commercial sources and used without further purification. Tetrabutylammonium hexafluorophosphate (TBAPF<sub>6</sub>) was recrystallized from hot ethanol and ferrocene was purified by sublimation before its use in cyclic voltammetry (CV) experiments. Progress of reactions was monitored by thin-layer chromatography using a Merck 60 F<sub>254</sub> precoated silica gel plate and visualized by short-wave ultraviolet light. Flash chromatography was performed with Silica Flash P60 silica gel (100–200 mesh).

### Physical Measurements

Absorption spectra were recorded using a LAB-INDIA UV/Vis Spectrophotometer UV 3000 in a UV cuvette of path length 10 mm fitted with a cap. The graphs are plotted using Originpro8. <sup>1</sup>H and <sup>13</sup>C {<sup>1</sup>H} NMR spectra are recorded on a Bruker 400 MHz spectrometer at the frequencies of 400 and 101 MHz, respectively. All chemical shifts are reported in parts per million (ppm) with respect to the <sup>1</sup>H (residual) chemical shifts of the d-solvent. The residual solvent signals are taken as the reference (CDCl<sub>3</sub>, 7.26 ppm for <sup>1</sup>H NMR spectra and

CDCl<sub>3</sub>, 77.16 ppm for <sup>13</sup>C NMR spectra). The signals observed are described as s (singlet), d (doublet), t (triplet), q (quartet), and m (multiplets). All coupling constants were reported in Hertz (Hz). High-resolution mass spectroscopy was performed on Waters Synapt-G2S, analyzer configuration Q-ToF with ion mobility and analyzed using Masslynx41. Cyclic voltammetry experiments were performed on a Keithley 2450 potentiostat. For the measurement, the electrode setup consisted of a glassy carbon working electrode, a Pt wire as the counter electrode, and Ag/Ag<sup>+</sup> (3 M KCl) as the reference electrode. Emission spectra were collected by a Fluoromax-4 (Horiba Jobin Yvon, NJ) spectrofluorophotometer. The analyte solution was placed in a quartz cuvette equipped with a screw cap having a path length of 10 mm.

## ASSOCIATED CONTENT

### Supporting Information

The Supporting Information is available free of charge at <https://pubs.acs.org/doi/10.1021/jacsau.3c00077>.

Experimental procedure; spectroscopic data; and NMR spectra for product molecules (PDF)

## AUTHOR INFORMATION

### Corresponding Author

**Debashis Adhikari** – Department of Chemical Sciences, Indian Institute of Science Education and Research Mohali, SAS Nagar 140306, India; [orcid.org/0000-0001-8399-2962](https://orcid.org/0000-0001-8399-2962); Email: [adhikari@iisermohali.ac.in](mailto:adhikari@iisermohali.ac.in)

### Authors

**Vikramjeet Singh** – Department of Chemical Sciences, Indian Institute of Science Education and Research Mohali, SAS Nagar 140306, India

**Rahul Singh** – Department of Chemical Sciences, Indian Institute of Science Education and Research Mohali, SAS Nagar 140306, India

**Arijit Singha Hazari** – Department of Chemistry, Stuttgart University, Stuttgart 70174, Germany

Complete contact information is available at: <https://pubs.acs.org/10.1021/jacsau.3c00077>

### Author Contributions

CRediT: **Vikramjeet Singh** conceptualization, data curation, investigation, methodology, validation; **Rahul Singh** data curation, validation; **Arijit Singha Hazari** data curation, investigation; **Debashis Adhikari** conceptualization, formal analysis, funding acquisition, validation, writing-original draft, writing-review & editing.

### Notes

The authors declare no competing financial interest.

## ACKNOWLEDGMENTS

We thank SERB (DST), India (Grant No. CRG/2021/001951), for financial support and IISER Mohali for seed grant. We thank Prof. Biprajit Sarkar (Univ. of Stuttgart) for spectroelectrochemistry measurement. V.S. thanks CSIR for a research fellowship, while R.S. thanks PMRF for the funding.

## REFERENCES

(1) Peris, E.; Crabtree, R. H. Key factors in pincer ligand design. *Chem. Soc. Rev.* **2018**, *47*, 1959–1968.

- (2) Alig, L.; Fritz, M.; Schneider, S. First-Row Transition Metal (De)Hydrogenation Catalysis Based On Functional Pincer Ligands. *Chem. Rev.* **2019**, *119*, 2681–2751.
- (3) Szabo, K. J.; Wendt, O. F. *Pincer and pincer-type complexes: applications in organic synthesis and catalysis*; John Wiley & Sons: 2014.
- (4) Ozerov, O. V. Rigid PNP Pincer ligands and Their Transition Metal Complexes. In *The Chemistry of Pincer Compounds*, Morales-Morales, D.; Jensen, C. M., Eds.; Elsevier: Amsterdam, 2007.
- (5) Eberhardt, N. A.; Guan, H. Reduction of CO<sub>2</sub> Mediated or Catalyzed by Pincer Complexes. In *Pincer Compounds: Chemistry and Applications*, Morales-Morales, D., Ed.; Elsevier: Amsterdam, 2018.
- (6) Ito, J.-I.; Nishiyama, H. Chiral Pincer Complexes for Asymmetric Reactions. In *Pincer Compounds: Chemistry and Applications*, Morales-Morales, D., Ed.; Elsevier: Amsterdam, 2018.
- (7) Roddick, D. M. Tuning of PCP Pincer Ligand Electronic and Steric Properties. In *Organometallic Pincer Chemistry*, van Koten, G.; Milstein, D., Eds.; Springer Berlin Heidelberg: Berlin, Heidelberg, 2013; pp. 49–88.
- (8) Valdés, H.; García-Eleno, M. A.; Canseco-Gonzalez, D.; Morales-Morales, D. Recent Advances in Catalysis with Transition-Metal Pincer Compounds. *ChemCatChem* **2018**, *10*, 3136–3172.
- (9) St. John, A.; Goldberg, K. I.; Heinekey, D. M. Pincer Complexes as Catalysts for Amine Borane Dehydrogenation. In *Organometallic Pincer Chemistry*, van Koten, G.; Milstein, D., Eds.; Springer Berlin Heidelberg: Berlin, Heidelberg, 2013; pp. 271–287.
- (10) Szabó, K. J. Pincer Complexes as Catalysts in Organic Chemistry. In *Organometallic Pincer Chemistry*, van Koten, G.; Milstein, D., Eds.; Springer Berlin Heidelberg: Berlin, Heidelberg, 2013; pp. 203–241.
- (11) Freeman, G. R.; Williams, J. A. G. Metal Complexes of Pincer Ligands: Excited States, Photochemistry, and Luminescence. In *Organometallic Pincer Chemistry*, van Koten, G.; Milstein, D., Eds.; Springer Berlin Heidelberg: Berlin, Heidelberg, 2013; pp. 89–129.
- (12) Poverenov, E.; Milstein, D. Noninnocent Behavior of PCP and PCN Pincer Ligands of Late Metal Complexes. In *Organometallic Pincer Chemistry*, van Koten, G.; Milstein, D., Eds.; Springer Berlin Heidelberg: Berlin, Heidelberg, 2013; pp. 21–47.
- (13) Khusnutdinova, J. R.; Milstein, D. Metal–Ligand Cooperation. *Angew. Chem., Int. Ed.* **2015**, *54*, 12236–12273.
- (14) Munhá, R. F.; Zarkesh, R. A.; Heyduk, A. F. Tuning the Electronic and Steric Parameters of a Redox-Active Tris(amido) Ligand. *Inorg. Chem.* **2013**, *52*, 11244–11255.
- (15) Haneline, M. R.; Heyduk, A. F. C–C Bond-Forming Reductive Elimination from a Zirconium(IV) Redox-Active Ligand Complex. *J. Am. Chem. Soc.* **2006**, *128*, 8410–8411.
- (16) Singh, K.; Kundu, A.; Adhikari, D. Ligand-Based Redox: Catalytic Applications and Mechanistic Aspects. *ACS Catal.* **2022**, *12*, 13075–13107.
- (17) Chmiel, A. F.; Williams, O. P.; Chernowsky, C. P.; Yeung, C. S.; Wickens, Z. K. Non-innocent Radical Ion Intermediates in Photo-redox Catalysis: Parallel Reduction Modes Enable Coupling of Diverse Aryl Chlorides. *J. Am. Chem. Soc.* **2021**, *143*, 10882–10889.
- (18) Pavlishchuk, V. V.; Addison, A. W. Conversion constants for redox potentials measured versus different reference electrodes in acetonitrile solutions at 25°C. *Inorg. Chim. Acta* **2000**, *298*, 97–102.
- (19) Arias-Rotondo, D. M.; McCusker, J. K. The photophysics of photoredox catalysis: a roadmap for catalyst design. *Chem. Soc. Rev.* **2016**, *45*, 5803–5820.
- (20) Wenger, O. S. Photoactive Complexes with Earth-Abundant Metals. *J. Am. Chem. Soc.* **2018**, *140*, 13522–13533.
- (21) Rehm, D.; Weller, A. Kinetics of Fluorescence Quenching by Electron and H-Atom Transfer. *Isr. J. Chem.* **1970**, *8*, 259–271.
- (22) Xu, J.; Cao, J.; Wu, X.; Wang, H.; Yang, X.; Tang, X.; Toh, R. W.; Zhou, R.; Yeow, E. K. L.; Wu, J. Unveiling Extreme Photoreduction Potentials of Donor–Acceptor Cyanoarenes to Access Aryl Radicals from Aryl Chlorides. *J. Am. Chem. Soc.* **2021**, *143*, 13266–13273.
- (23) Zhao, Y.; Truhlar, D. G. The M06 suite of density functionals for main group thermochemistry, thermochemical kinetics, non-covalent interactions, excited states, and transition elements: two new functionals and systematic testing of four M06-class functionals and 12 other functionals. *Theor. Chem. Acc.* **2008**, *120*, 215–241.
- (24) Shon, J.-H.; Kim, D.; Rathnayake, M. D.; Sittel, S.; Weaver, J.; Teets, T. S. Photoredox catalysis on unactivated substrates with strongly reducing iridium photosensitizers. *Chem. Sci.* **2021**, *12*, 4069–4078.
- (25) Mfuh, A. M.; Doyle, J. D.; Chhetri, B.; Arman, H. D.; Larionov, O. V. Scalable, Metal- and Additive-Free, Photoinduced Borylation of Haloarenes and Quaternary Arylammonium Salts. *J. Am. Chem. Soc.* **2016**, *138*, 2985–2988.
- (26) Qiao, Y.; Yang, Q.; Schelter, E. J. Photoinduced Miyaura Borylation by a Rare-Earth-Metal Photoreductant: The Hexachloroacetate(III) Anion. *Angew. Chem., Int. Ed.* **2018**, *57*, 10999–11003.
- (27) Cybularczyk-Cecotka, M.; Szczepanik, J.; Giedyk, M. Photocatalytic strategies for the activation of organic chlorides. *Nat. Catal.* **2020**, *3*, 872–886.
- (28) Koike, T.; Akita, M. Visible-light radical reaction designed by Ru- and Ir-based photoredox catalysis. *Inorg. Chem. Front.* **2014**, *1*, 562–576.
- (29) Blanksby, S. J.; Ellison, G. B. Bond Dissociation Energies of Organic Molecules. *Acc. Chem. Res.* **2003**, *36*, 255–263.
- (30) Wertjes, W. C.; Wolfe, L. C.; Waller, P. J.; Kalyani, D. Nickel or Phenanthroline Mediated Intramolecular Arylation of sp<sup>3</sup> C–H Bonds Using Aryl Halides. *Org. Lett.* **2013**, *15*, 5986–5989.
- (31) Wagner, A. M.; Hickman, A. J.; Sanford, M. S. Platinum-Catalyzed C–H Arylation of Simple Arenes. *J. Am. Chem. Soc.* **2013**, *135*, 15710–15713.
- (32) Gensch, T.; Hopkinson, M. N.; Glorius, F.; Wencel-Delord, J. Mild metal-catalyzed C–H activation: examples and concepts. *Chem. Soc. Rev.* **2016**, *45*, 2900–2936.
- (33) Wedi, P.; Farizyan, M.; Bergander, K.; Mück-Lichtenfeld, C.; van Gemmeren, M. Mechanism of the Arene-Limited Nondirected C–H Activation of Arenes with Palladium. *Angew. Chem., Int. Ed.* **2021**, *60*, 15641–15649.
- (34) Degorce, S. L.; Bodnarchuk, M. S.; Scott, J. S. Lowering Lipophilicity by Adding Carbon: AzaSpiroHeptanes, a logD Lowering Twist. *ACS Med. Chem. Lett.* **2019**, *10*, 1198–1204.
- (35) Dai, P.; Ma, J.; Huang, W.; Chen, W.; Wu, N.; Wu, S.; Li, Y.; Cheng, X.; Tan, R. Photoredox C–F Quaternary Annulation Catalyzed by a Strongly Reducing Iridium Species. *ACS Catal.* **2018**, *8*, 802–806.
- (36) Zhou, F.; Liu, Y.-L.; Zhou, J. Catalytic Asymmetric Synthesis of Oxindoles Bearing a Tetrasubstituted Stereocenter at the C-3 Position. *Adv. Synth. Catal.* **2010**, *352*, 1381–1407.
- (37) Marti, C.; Carreira, E. M. Construction of Spiro[pyrrolidine-3,3'-oxindoles] – Recent Applications to the Synthesis of Oxindole Alkaloids. *Eur. J. Org. Chem.* **2003**, *2003*, 2209–2219.
- (38) Hibino, S.; Choshi, T. Simple indole alkaloids and those with a nonrearranged monoterpenoid unit. *Nat. Prod. Rep.* **2001**, *18*, 66–87.
- (39) Chen, J.-Q.; Wei, Y.-L.; Xu, G.-Q.; Liang, Y.-M.; Xu, P.-F. Intramolecular 1,5-H transfer reaction of aryl iodides through visible-light photoredox catalysis: a concise method for the synthesis of natural product scaffolds. *Chem. Commun.* **2016**, *52*, 6455–6458.
- (40) Nguyen, J. D.; Tucker, J. W.; Konieczynska, M. D.; Stephenson, C. R. J. Intermolecular Atom Transfer Radical Addition to Olefins Mediated by Oxidative Quenching of Photoredox Catalysts. *J. Am. Chem. Soc.* **2011**, *133*, 4160–4163.
- (41) Maji, T.; Karmakar, A.; Reiser, O. Visible-Light Photoredox Catalysis: Dehalogenation of Vicinal Dibromo-,  $\alpha$ -Halo-, and  $\alpha,\alpha$ -Dibromocarbonyl Compounds. *J. Org. Chem.* **2011**, *76*, 736–739.
- (42) Pham, P. V.; Nagib, D. A.; MacMillan, D. W. C. Photoredox Catalysis: A Mild, Operationally Simple Approach to the Synthesis of  $\alpha$ -Trifluoromethyl Carbonyl Compounds. *Angew. Chem., Int. Ed.* **2011**, *50*, 6119–6122.
- (43) MacKenzie, I. A.; Wang, L.; Onuska, N. P. R.; Williams, O. F.; Begam, K.; Moran, A. M.; Dunitz, B. D.; Nicewicz, D. A. Discovery

and characterization of an acridine radical photoreductant. *Nature* **2020**, *580*, 76–80.

(44) Deprez, P.; Guillaume, J.; Becker, R.; Corbier, A.; Didierlaurent, S.; Fortin, M.; Frechet, D.; Hamon, G.; Heckmann, B.; Heitsch, H. Sulfonylureas and Sulfonylcarbamates as New Non-Tetrazole Angiotensin II Receptor Antagonists. Discovery of a Highly Potent Orally Active (Imidazolylbiphenyl)sulfonylurea (HR 720). *J. Med. Chem.* **1995**, *38*, 2357–2377.

(45) Dey, D.; Kundu, A.; Roy, M.; Pal, S.; Adhikari, D. Aromatization as the driving force for single electron transfer towards C–C cross-coupling reactions. *Catal. Sci. Technol.* **2022**, *12*, 1934–1940.

(46) Cahard, E.; Schoenebeck, F.; Garnier, J.; Cutulic, S. P. Y.; Zhou, S.; Murphy, J. A. Electron Transfer to Benzenes by Photoactivated Neutral Organic Electron Donor Molecules. *Angew. Chem., Int. Ed.* **2012**, *51*, 3673–3676.

(47) Doni, E.; Murphy, J. A. Evolution of neutral organic super-electron-donors and their applications. *Chem. Commun.* **2014**, *50*, 6073–6087.

(48) Schmidt, V. A.; Quinn, R. K.; Brusoe, A. T.; Alexanian, E. J. Site-Selective Aliphatic C–H Bromination Using N-Bromoamides and Visible Light. *J. Am. Chem. Soc.* **2014**, *136*, 14389–14392.

(49) Shields, B. J.; Doyle, A. G. Direct C(sp<sup>3</sup>)–H Cross Coupling Enabled by Catalytic Generation of Chlorine Radicals. *J. Am. Chem. Soc.* **2016**, *138*, 12719–12722.

(50) Sharma, A.; Hartwig, J. F. Metal-catalysed azidation of tertiary C–H bonds suitable for late-stage functionalization. *Nature* **2015**, *517*, 600–604.

(51) Morcillo, S. P.; Dauncey, E. M.; Kim, J. H.; Douglas, J. J.; Sheikh, N. S.; Leonori, D. Photoinduced Remote Functionalization of Amides and Amines Using Electrophilic Nitrogen Radicals. *Angew. Chem., Int. Ed.* **2018**, *57*, 12945–12949.

(52) Ghosh, I.; Shaikh, R. S.; König, B. Sensitization-Initiated Electron Transfer for Photoredox Catalysis. *Angew. Chem., Int. Ed.* **2017**, *56*, 8544–8549.

(53) Ghosh, I.; Ghosh, T.; Bardagi, J. I.; König, B. Reduction of aryl halides by consecutive visible light-induced electron transfer processes. *Science* **2014**, *346*, 725–728.

(54) Ghosh, I.; König, B. Chromoselective Photocatalysis: Controlled Bond Activation through Light-Color Regulation of Redox Potentials. *Angew. Chem., Int. Ed.* **2016**, *55*, 7676–7679.